MOLECULAR AND CELLULAR BIOLOGY, Nov. 1992, p. 5004–5014
0270-7306/92/115004-11$02.00/0

Vol. 12, No. 11

Effects of Histone Acetylation on Chromatin Topology In Vivo

LEONARD C. LUTTER,[1]* LUANN JUDIS,[1] AND ROBERT F. PARETTI[2]

Molecular Biology Research Program, Henry Ford Hospital, 2799 West Grand Boulevard, Detroit, Michigan 48202,[1] and Biophysics Research Division, University of Michigan, 2200 Bonisteel Boulevard, Ann Arbor, Michigan 48109[2]

Received 27 July 1992/Accepted 5 August 1992

Recently a model for eukaryotic transcriptional activation has been proposed in which histone hyperacetylation causes release of nucleosomal supercoils, and this unconstrained tension in turn stimulates transcription (V. G. Norton, B. S. Imai, P. Yau, and E. M. Bradbury, Cell 57:449–457, 1989; V. G. Norton, K. W. Marvin, P. Yau, and E. M. Bradbury, J. Biol. Chem. 265:19848–19852, 1990). These studies analyzed the effect of histone hyperacetylation on the change in topological linking number which occurs during nucleosome assembly in vitro. We have tested this model by determining the effect of histone hyperacetylation on the linking number change which occurs during assembly in vivo. We find that butyrate treatment of cells infected with simian virus 40 results in hyperacetylation of the histones of the extracted viral minichromosome as expected. However, the change in constrained supercoils of the minichromosome DNA is minimal, a result which is inconsistent with the proposed model. These results indicate that the proposed mechanism of transcriptional activation is unlikely to take place in the cell.

It is well established that DNA in prokaryotes is negatively supercoiled and that these supercoils are unconstrained (21, 36, 48, 61). The magnitude of this unconstrained supercoiling is regulated by DNA topoisomerases, and variation in the level of supercoiling is known to regulate transcription of certain genes. The situation in eukaryotes is less clear (22, 23). Eukaryotic DNA is supercoiled, but these supercoils are constrained by the nucleosomes for most of the DNA. However, since only a small fraction of the eukaryotic genome is transcriptionally active at any one time in a given cell, it remains possible that the DNA of this transcribed chromatin, like the DNA of prokaryotes, contains unconstrained supercoiling. Indeed, numerous studies have argued that the transcriptionally active chromatin contains totally unconstrained supercoils (39–41, 56). However, these studies were all correlative, and when direct analyses of the topology of transcribing chromatin were carried out, it was found that transcribed chromatin contains constrained supercoiling in an amount consistent with typical nucleosomal organization (4, 10, 11, 43, 52).

While totally unconstrained supercoils are not a property of transcribed eukaryotic genes, there remains the possibility that some level of unconstrained supercoiling is important for gene activation. However, while the enzyme DNA gyrase can introduce unconstrained supercoiling into prokaryotic DNA, a eukaryotic version of this enzyme has yet to be identified. This raises a question as to the origin of this putative unconstrained tension in the transcribed chromatin. One source of unconstrained supercoils could be the constrained supercoils already present in the nucleosome. For example, if a nucleosomase were to partially or completely destroy a selected nucleosome's ability to constrain the equivalent of one supercoil, that supercoil would then be released as an unconstrained supercoil (see, e.g., reference 64). This in turn could cause, for example, a DNA structural transition elsewhere in the domain which would be important for transcriptional activation. Thus, the nucleosome itself could be a component of a DNA gyrase when it acts in concert with the hypothetical nucleosomase.

Such a utilization of nucleosomal supercoils is a feature of a model for eukaryotic gene activation proposed recently by Norton et al. (49, 50). As in the models discussed above, the authors propose that unconstrained supercoiling is important for regulation of transcription. They further propose the nucleosome as the source of this unconstrained topological tension, with histone hyperacetylation causing the release of part of the constrained nucleosomal supercoils. This proposal derives from their analysis of the effect of histone hyperacetylation on the extent of topological change caused by nucleosome assembly in vitro. They find that nucleosomes containing hyperacetylated histones induce a lower level of negative supercoiling than do those containing normally acetylated histones; the linking number change (ΔL) is -1.0 per nucleosome for the normally acetylated sample but -0.8 per nucleosome for the hyperacetylated sample. Citing literature that correlates high levels of histone acetylation with transcriptionally active chromatin (1, 16), they propose that the process of hyperacetylation of nucleosomal histones provides the gyraselike activity to introduce unconstrained supercoiling into the domain of a gene to be activated. Thus, the histones of the chromatin of a gene to be activated are hyperacetylated, which releases 0.2 negative supercoil per nucleosome into the topological domain, and this now unconstrained supercoiling in turn causes changes such as critical DNA structural transitions which result in transcriptional activation.

The experiments of Norton et al. (49) quantify the topological effects of histone hyperacetylation in an in vitro reconstitution system. Their model predicts that in the cell, the constrained supercoiling of a minichromosome containing highly acetylated histones should be 20% less than that of a minichromosome containing normal histones.

In this study, we tested this model by analyzing the effect of histone hyperacetylation on in vivo-assembled minichromosomes of both simian virus 40 (SV40) and transfected

* Corresponding author.

plasmids. We find that induction of histone hyperacetylation by addition of butyrate to the culture medium does not cause the level of constrained supercoils to drop by the predicted 20%; rather, there is little if any topological effect. This finding demonstrates that the effects of histone acetylation in vitro do not in fact occur on chromatin assembled in vivo. These results argue against the model proposing transcriptional activation via acetylation-induced unconstrained supercoiling.

MATERIALS AND METHODS

Cells, virus, and nuclear extract preparation. Growth of cells (BS-C-1 and COS7, both from the American Type Culture Collection), infection with SV40 (strain 776), and electroporation procedures have been described previously (4, 24, 43, 52). Isotonic nuclear extract was prepared by a modification of a previously described procedure (43). Briefly, cells were scraped in TD buffer (38) from plates 48 h after infection or electroporation and lysed by suspension in the same buffer containing 0.5% Nonidet P-40 but also including protease inhibitors (0.2 mM phenylmethylsulfonyl fluoride [Sigma], 5 μg of pepstatin A [Sigma] per ml, 5 μg of leupeptin [Boehringer] per ml, and 10 μg of aprotinin [Sigma] per ml). Final nuclear extract was prepared by resuspension of the nuclear pellet in TL buffer (137 mM NaCl, 5.1 mM KCl, 1 mM Na_2EDTA, 50 mM Tris-HCl [pH 7.9]) (43) to which was added the protease inhibitors described above (TLI buffer). Resuspension volume was 0.05 ml/15-cm culture plate. When indicated, sodium butyrate was added as a 1 M stock to the culture medium to give a final concentration of 15 mM (54). Sodium butyrate (15 mM) was included in all preparation buffers in samples from butyrate-treated cells.

Topoisomerase incubations and topoisomer analysis. Nuclear extract or nuclei were incubated with either calf thymus (Bethesda Research Laboratories) or wheat germ (Promega) topoisomerase I for the specified times at 8 U (Promega) per 10^6 cells equivalent of nuclear extract or nuclei (43). Heparin (1 mg/ml; Sigma) was then added to inhibit topoisomerase and dissociate histones from the DNA (4). For some experiments, nuclear extract was fractionated directly by electrophoresis in an agarose gel after addition of sample buffer (final concentrations, 5% glycerol, 0.2% bromphenol blue, and 0.2% xylene cyanol). For transcription complex/ternary complex analysis, ternary complexes were radioactively labeled by run-on extension in vitro and analyzed as described previously (4, 43). When whole nuclei were analyzed, reactions were stopped with 1% lithium dodecyl sulfate. This procedure allows termination of the 0°C incubations without detergent precipitation. Samples were then processed according to the method of Hirt (28). Electrophoresis was carried out in an agarose gel (0.7%) in TBE buffer (44) containing 15.5 μg of chloroquine diphosphate (Sigma) per ml to separate the negatively supercoiled DNA as a series of positively supercoiled topoisomers in the gel (43). Southern analysis of plasmid DNA was done as described previously (4).

Densitometry and topoisomer distribution center location were performed as described previously (43), with some modifications. In addition to use of a manual procedure (2) for fitting a Gaussian distribution to the data, some of the data sets (e.g., Fig. 1d and e and Fig. 4c and d) were fitted by using the curve-fitting option of the Sigmaplot 4.1 graphics package (Jandel Scientific). The two procedures produced results which were virtually identical. Finally, some of the data sets were also analyzed by plotting $i^{-1}\ln[(\alpha_m + i)(\alpha_m)^{-1}]$ versus i (18, 46). Both butyrate-treated and control samples produced linear plots with correlation coefficients (r^2) of >0.95. The results of these analyses were also used to calculate values for *NK* given in the legends for Fig. 1d and e and Fig. 4c and d.

Size exclusion chromatography. Nuclear extract from five 15-cm plates was made 0.45 M NaCl by addition of 5 M NaCl with stirring (42), after which it was fractionated on Bio-Gel A-5m (7-ml column) equilibrated with 0.45 M NaCl, 1 mM EDTA, and 50 mM Tris-HCl (pH 7.9). The void volume, which contains the minichromosomes, was located via A_{260}, and the peak was pooled. A sample of this pool was passed over Sephadex G-50 equilibrated in TL buffer, and this sample was incubated with topoisomerase as described above for topology analysis. The remainder of the Bio-Gel pool was precipitated with trichloroacetic acid for histone analysis as described below. Butyrate (15 mM) was included in all buffers for the butyrate-treated samples.

Histone analysis. Histones were analyzed by electrophoresis in acrylamide gels containing sodium dodecyl sulfate (SDS) as described previously (20). For electrophoresis under acid-urea conditions (51), samples were first precipitated by addition of one-quarter volume of trichloroacetic acid (1 g/ml), then washed with acidified acetone (1 ml of concentrated HCl per 100 ml of acetone) and acetone (5), and dried under vacuum. Samples were then resuspended in 8 M urea–0.2% methyl green–5 mg of protamine sulfate (Sigma) per ml (57). Electrophoresis was performed at 18 V/cm until the blue component of the methyl green reached the bottom of the gel (27). The gel was then stained with 0.1% Coomassie blue R250 in methanol-acetic acid-water (5:5:1) and destained in 10% acetic acid–25% methanol (27). Densitometry was carried out on the stained gel directly, using an LKB Ultroscan II densitometer. Analysis of control nuclear extract immediately after isolation showed an elevated histone acetylation level as described previously (12, 33, 57), but histone deacetylase activity present in the nuclear extract reduced this level during processing to the levels shown in Fig. 1 and 3.

Electron microscopy. SV40 nuclear extracts were passed over Sepharose 4B equilibrated with 2 mM triethanolamine-HCl (pH 8.0) and 0.2 mM EDTA. The void volume peak was diluted to 0.2 μg of DNA per ml with column buffer and fixed on ice with 0.4% formaldehyde (Pelco 16% aqueous) for 8 h and 0.4% glutaraldehyde (Pelco 8% aqueous) for 6 h. Copper electron microscope grids (400 mesh) were coated with a carbon film and rendered hydrophilic by treatment with Alcian blue (Serva 8GX) (34). Aliquots (10 μl) of fixed SV40 were placed on a silicone grid pad, after which a grid was inverted on each drop for 5 min. The grids were washed twice with water (3 min per wash) and once with 100% ethanol (10 s), air dried, and rotary shadowed at 7° with 80:20 Pt-Pd.

A Zeiss EM 902 was used for microscopy. Suitable molecules were photographed at ×30,000 magnification. The only selection criterion was that the SV40 molecule not be folded upon itself. Objectivity was enhanced by obtaining the samples blind; i.e., the microscopist did not know which sample was control and which was butyrate treated. The nucleosomes on each molecule were counted from numbered prints at ×100,000 magnification.

RESULTS

Effect of butyrate on SV40 minichromosome topology. SV40 has proven to be a very useful model for characterization of

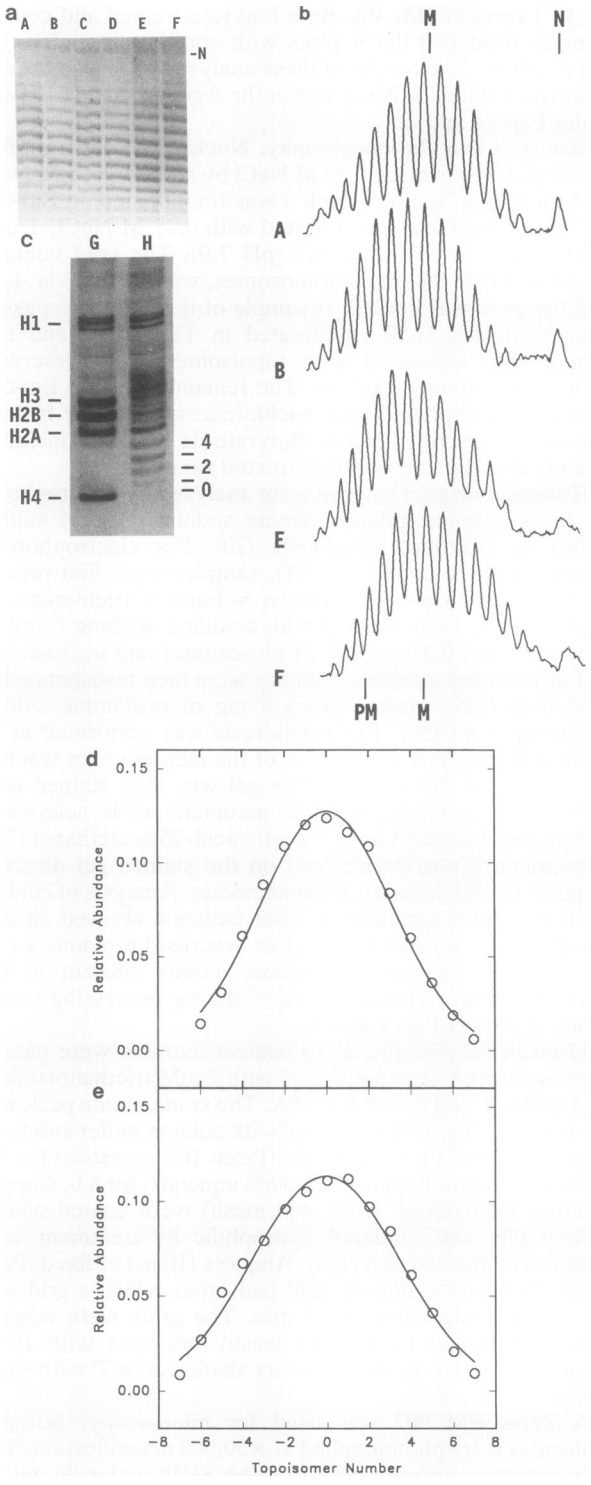

FIG. 1. DNA topology of SV40 minichromosomes isolated from cells grown in the presence of butyrate. BS-C-1 cells were infected with SV40 and harvested 48 h later. Sodium butyrate (15 mM) was added to the medium at various times (listed below) prior to harvest. An isotonic nuclear extract was prepared at harvest. Samples were incubated with calf thymus topoisomerase I at 37°C for 30 min, after which some of the samples were transferred to 0°C and incubated for a further 24 h. Heparin was added to inhibit topoisomerase activity and to generate ternary complexes, after which in vitro run-on transcription was carried out to label the ternary complexes. The samples were then fractionated by electrophoresis in a 0.7% agarose gel containing 15.5 μg of chloroquine phosphate per ml (see Materials and Methods). This concentration of chloroquine is sufficient to cause the negatively supercoiled topoisomers of SV40 DNA to migrate as positively supercoiled topoisomers in the gel (4, 43). Thus, an increasing mobility in this gel corresponds to an increasing linking number in the DNA or a decreasing level of negative supercoiling in the original sample. Following electrophoresis, the gel was stained with ethidium bromide and photographed under UV light. Panel a shows a photograph of the negative of the stained gel; panel b shows densitometric scans of selected lanes. Samples: A, no butyrate treatment, extract incubated at 37°C only; B, no butyrate treatment, extract incubated at 0°C; C, butyrate added to cells 6 h before harvest, extract incubated at 37°C only; D, butyrate added to cells 6 h before harvest, extract incubated at 0°C; E, butyrate added to cells 12 h before harvest, extract incubated at 0°C; F, butyrate added to cells 12 h before harvest, extract incubated at 37°C only. N in panel a indicates the mobility of the nicked DNA; M above the scans indicates the mean mobility of the topoisomer distribution of sample A; M below the scans indicates the mean mobility of the topoisomer distribution of sample F; PM indicates the location of the predicted mean mobility of sample F according to Norton et al. (49, 50), as described in the text. (c) Histone content of SV40 minichromosomes in the nuclear extract, determined by electrophoresis in an acrylamide gel in the presence of acetic acid and urea (see Materials and Methods). Samples: G, histones isolated from nuclear extract of untreated cells; H, histones isolated from nuclear extract of cells grown in the presence of butyrate for 12 h before harvest. The mobilities of the various histones are identified (H1, H2A, H2B, H3, and H4), as are the mobilities of the species of histone H4 carrying increasing numbers of acetyl groups (none to four). (d and e) Gaussian curves fitted by computer to topoisomer distribution data for samples B (d) and E (e). The circles represent the intensities of the various topoisomer bands; 0 is assigned to the maximum intensity topoisomer in the 0°C control (sample B). The solid line is the computer-generated fit to the data. Note that the top of the gel corresponds to the left of the panel. The means and standard deviations about the mean are -0.1 ± 0.7 and 3.13 ± 0.06 for panel d and -0.6 ± 0.9 and 3.51 ± 0.07 for panel e. Linear graphical analyses (18, 46) were also performed on these data; the correlation coefficient r^2 was greater than 0.97 in each case. Estimation of NK from these analyses gave values of 276RT and 240RT for panels d and e, respectively.

the topology of chromatin DNA. We used this system to test whether the levels of constrained supercoils are different for minichromosomes isolated from cells grown in the presence and absence of sodium butyrate. Butyrate has been shown to increase the level of histone hyperacetylation by inhibiting histone deacetylases (3, 9, 14, 16, 26, 55, 58).

BS-C-1 cells were infected with SV40, and sodium butyrate was added to the medium for various times before harvest. Nuclear extracts containing SV40 minichromosomes were then prepared. Such extracts contain the majority of the SV40 minichromosomes but virtually no cellular chromatin (25). Electrophoretic analysis of the histones of the minichromosomes in the nuclear extract (Fig. 1c) demonstrated that butyrate treatment of the cells markedly increased histone hyperacetylation of histone H4 as well as of histones H2B and H3; these results are consistent with numerous studies on cellular histones (9, 13, 49, 63). Densitometry revealed that the net increase of acetylation resulting from butyrate treatment ranged from 3.0 to 3.6 acetyl groups per H4 (see also Fig. 3e, scan H).

To quantitate constrained supercoils in the minichromosomes, nuclear extract samples were incubated with topoisomerase I. Heparin was then added to remove the histones, and the DNA was fractionated by electrophoresis in an agarose gel in the presence of chloroquine (Fig. 1a). The series of bands in each lane represents the series of topoiso-

TABLE 1. Linking number change induced by butyrate treatment

Sample	Temp (°C) relaxed at[a]	Predicted value[b]	Observed value[c] (avg ± SD)
SV40			
Hirt extract			
L_{6h}–L_{0h}[d]			0.05 ± 0.05 (2)
L_{12h}–L_{0h}			−0.25 ± 0.15 (2)
Nuclear extract			
L_{6h}–L_{0h}	0		0.07 ± 0.12 (3)
L_{6h}–L_{0h}	37		−0.07 ± 0.31 (3)
L_{12h}–L_{0h}	0		−0.06 ± 1.05 (4)
L_{12h}–L_{0h}	37		−0.52 ± 0.49 (8)
		+4.8	−0.53 ± 0.67 (12)[e]
Column purified[f]			
L_{12h}–L_{0h}	37	+4.8	−0.53 ± 0.31 (3)
$L_{0.45M}$–$L_{0.14M}$[g]	37		−0.91 ± 0.28 (4)
VTC			
L_{12h}–L_{0h}	0		−0.63 ± 0.68 (2)
L_{12h}–L_{0h}	37		−0.73 ± 0.69 (2)
			−0.68 ± 0.64 (4)[e]
pORAS7, nuclei			
L_{12h}–L_{0h}	0		−1.4 ± 0.2 (2)
L_{12h}–L_{0h}	37		−1.65 ± 0.15 (2)
		+7.4	−1.5 ± 0.3 (4)[e]

[a] Temperature at which the incubation with topoisomerase was carried out.
[b] Linking number change calculated according to the proposal of Norton et al. (49, 50) that histone hyperacetylation causes a linking number change of +0.2 per nucleosome, i.e., about a 20% decrease in the level of negative supercoiling. SV40 contains 24 nucleosomes and 1.0 negative supercoil per nucleosome (29, 60), so (+0.2/nucleosome) × (24 nucleosomes) = +4.8. Plasmid pORAS7 contains 7,000 bp of DNA, and there are 188 bp per nucleosome (59), so (7,000/188) × (+0.2/nucleosome) = +7.4.
[c] Number of determinations is given in parentheses.
[d] Subscript denotes the length of time the cells were treated with butyrate prior to harvest. Thus, the untreated control sample is designated 0 h.
[e] Average of both the 0 and 37°C values.
[f] This sample was passed over a Bio-Gel A-5m column in the presence of 0.45 M NaCl prior to incubation (see text).
[g] Linking number difference between the column-purified sample (0.45 M) and the original, unpurified nuclear extract sample (0.14 M) following relaxation of both at 0.14 M NaCl.

mers of the circular SV40 molecules, with adjacent bands representing topoisomers which differ by a linking number of 1 (15, 29). The center of each distribution of topoisomers represents the mean linking number for that distribution, so a difference in the mean linking numbers of two samples is seen as a difference in mobilities of the centers of the two topoisomer distributions. Under the electrophoresis conditions used for Fig. 1, lower mobility corresponds to a lower linking number; for reference, this value would be expressed as an increased level of negative supercoiling under normal solution conditions. The centers of the topoisomer distributions were determined by analysis of the densitometer scans of the photographic negative; the scans are shown in Fig. 1b. The envelope of the distribution is Gaussian, as seen in (Fig. 1d and e).

If the butyrate-induced histone hyperacetylation causes a 20% decrease in nucleosomal supercoiling as proposed by Norton et al. (49), then the center of the topoisomer distribution of the butyrate-treated sample should be expected to exhibit a mobility equivalent to about 4.8 topoisomer bands further down the gel than the center of the distribution of the untreated sample. It can be seen in Fig. 1 that this is not the case. The M beneath the densitometer scans marks the center of the topoisomer distribution of the sample treated for 12 h with butyrate and incubated with topoisomerase at 37°C (Fig. 1b, scan F); it corresponds to the mean linking number of that distribution. The M at the top of Fig. 1b marks the mean of the distribution of the sample which was prepared from cells which were not treated with butyrate (Fig. 1b, scan A). A comparison of the centers of the two distributions shows that they are in fact quite close to each other, differing by less than one linking number equivalent. In contrast, the proposal of Norton et al. (49) would predict that the center of the distribution for the butyrate-treated sample should be located considerably further down the gel (4.8 bands), at the position marked PM (Fig. 1b, scan F). Clearly the predicted shift did not occur. A similar lack of mobility shift resulted when the topoisomer treatment was performed at 0°C (Fig. 1a, lane B versus lane E). The difference between the respective 0 and 37°C values (lane A versus lane B, lane C versus lane D, and lane E versus lane F) demonstrates that the topoisomerase was in fact active on the minichromosome (cf. reference 43), meaning that unconstrained supercoils would have been removed when present. Data from a series of such experiments, including butyrate treatments of 12 and 6 h, are summarized in Table 1 (SV40, nuclear extract). The results show that butyrate treatment in vivo caused little if any topological change, a result which contrasts markedly with the prediction of Norton et al. (49) of 4.8 fewer negative supercoils.

Effect of butyrate on the topology of the SV40 viral transcription complex. The experiment shown in Fig. 1 also included an examination of the effect of butyrate on the SV40 viral transcription complex (VTC) topology, the results of which are shown in Fig. 2. VTC are also present in the nuclear extract but in a much lower amount (about 1% of the bulk minichromosomes). Nevertheless, it is possible to quantitate changes in VTC topology by analyzing the transcriptional ternary complex by the same agarose gel electrophoresis method (4, 10, 11, 43, 52). The ternary complex is composed of transcription complex DNA, engaged RNA polymerase II which was initiated in the cell, and nascent

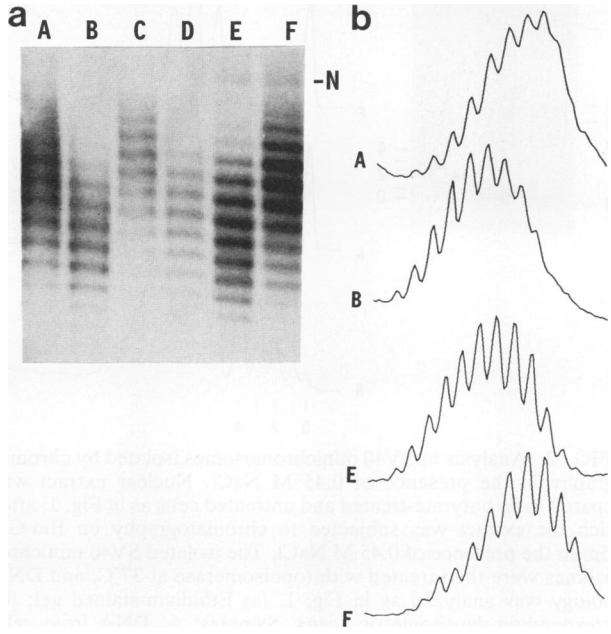

FIG. 2. Topology of SV40 VTC DNA from cells grown in the presence of butyrate. (a) Autoradiograph of the gel shown in Fig. 1a; (b) corresponding densitometric scans. Channels are labeled as in Fig. 1.

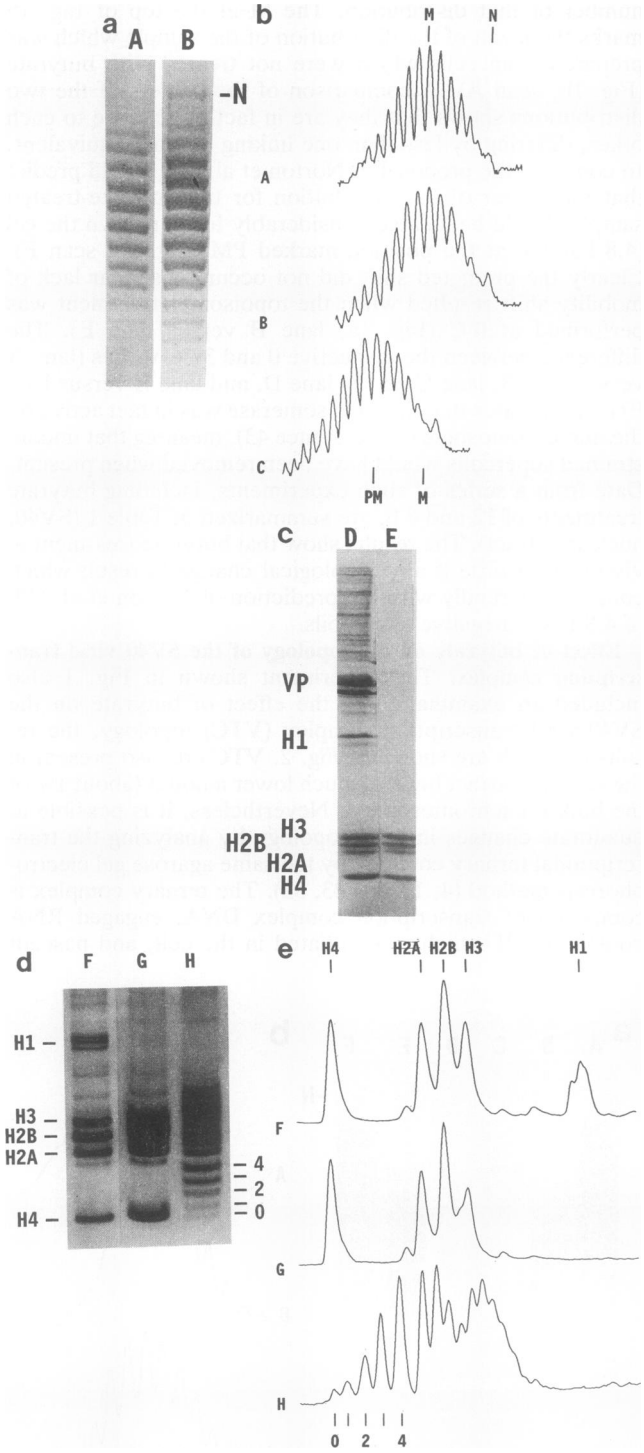

FIG. 3. Analysis of SV40 minichromosomes isolated by chromatography in the presence of 0.45 M NaCl. Nuclear extract was prepared from butyrate-treated and untreated cells as in Fig. 1, after which the extract was subjected to chromatography on Bio-Gel A-5m in the presence of 0.45 M NaCl. The isolated SV40 minichromosomes were then treated with topoisomerase at 37°C, and DNA topology was analyzed as in Fig. 1. (a) Ethidium-stained gel; (b) corresponding densitometric scans. Samples: A, DNA from cells not treated with butyrate; B, DNA from cells grown in the presence of butyrate for 12 h prior to harvest. M above the scans marks the mean mobility of the topoisomer distribution of sample A; M below the scans marks the mean for sample B; PM marks the predicted mean for sample B according to the model of Norton et al. (49, 50). Scan C is scan B moved to the left so that its mean coincides with the predicted mean; thus, scan C provides an example of what scan B should have looked like if the proposal of Norton et al. (49, 50) described the behavior of minichromosomes assembled in vivo. (c) Separation of protein samples by electrophoresis in a polyacrylamide gel in the presence of SDS. Samples: D, nuclear extract from untreated cells; E, minichromosomes isolated from untreated cells by chromatography as described above. The mobilities of histones (H1, H3, H2B, H2A, and H4) as well as the SV40 virion proteins (VP) are shown. (d) Separation of protein samples by electrophoresis in a polyacrylamide gel in the presence of acetic acid-urea as in Fig. 1. Sources of samples: F, nuclear extract from untreated cells; G, minichromosomes isolated from untreated cells by chromatography as described above; H, as G only from cells treated with butyrate for 12 h prior to harvest. Histone mobilities are indicated at the left, and the number of acetyl groups per H4 is indicated at the right. The relative loadings of samples G and H are greater than that of sample F in order to emphasize the extent of removal of histone H1. (e) Scans of samples F through H.

RNA. The complex can be labeled by run-on transcription in vitro by using [^{32}P]UTP, and it separates as a series of topoisomers during agarose gel electrophoresis.

After the topoisomerase incubations were performed in the experiment shown in Fig. 1, the topoisomerase was inactivated by the addition of heparin. Then run-on transcription in the presence of [^{32}P]UTP was carried out prior to electrophoresis. As described above and shown in Fig. 1, the photograph of the ethidium-stained gel reveals the topoisomer distributions of the bulk minichromosomes of the various samples. Following the photography, the gel was dried and autoradiographed. The autoradiograph, shown in Fig. 2a for the same gel shown in Fig. 1a, reveals the topoisomer distributions of the transcription complexes in the same nuclear extract samples.

A comparison of lanes B and E in Fig. 2a reveals that the butyrate treatment also has a minimal effect on the level of constrained supercoiling in the VTC. This is true whether the topoisomerase treatment was carried out at 0°C (lane B versus lane E) or 37°C (lane A versus lane F). Again, the difference in the 0 and 37°C values for the same sample of extract (compare lanes A and B, C and D, and E and F) demonstrates that the topoisomerase relaxed unconstrained supercoils in the VTC (43). The average value of several experiments (Table 1, SV40, VTC) reveals that the butyrate effect on the VTC topology was virtually the same as its effect on SV40 bulk minichromosome topology; butyrate caused little change in the topology of the DNA of either complex and, if anything, caused them to become a fraction of a turn more negatively supercoiled. This lack of effect of butyrate on the topology of the transcription complex is one prediction (49) which was in fact observed; i.e., it has been proposed that the transcription complex already has hyperacetylated histones (1, 49), so no significant further increase in acetylation would be expected with butyrate treatment. Therefore, no change in linking number would be predicted. However, what would be predicted is a difference between the bulk minichromosomes (transcriptionally inactive) and the transcription complex, and this was not observed. Another expectation (1) is that butyrate might increase the specific activity of transcription of the minichromosomes by recruiting more minichromosomes into VTC, but a comparison of ratios of densitometer peak heights in corresponding channels of Fig. 1 and 2 showed no systematic increase in

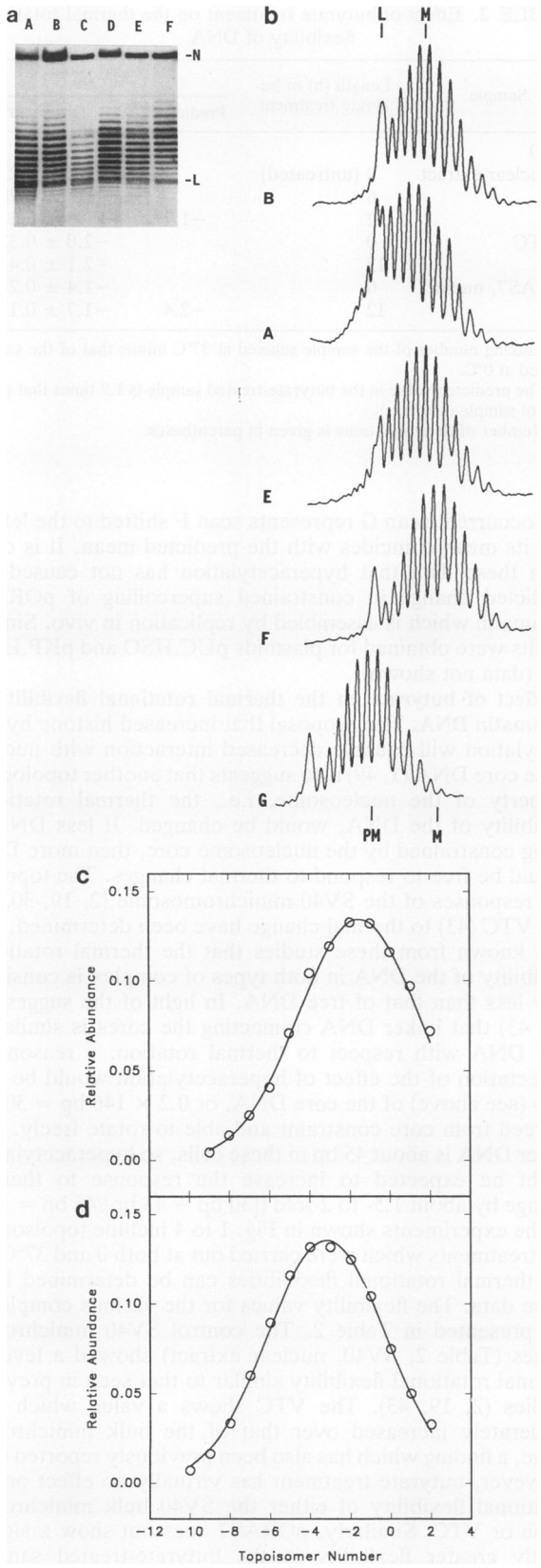

FIG. 4. Topology of minichromosomes of transfected plasmids. Plasmid pORAS7 was transfected into COS7 cells, and nuclei were prepared 48 h later. Topoisomerase was added to the nuclei, and incubation was carried out at 37°C for 30 min. Some of the samples were then incubated for an additional 12 h at 0°C. Incubation reactions were stopped by the addition of lithium dodecyl sulfate at the appropriate temperature. The extracted DNA was then fractionated by electrophoresis as in Fig. 1, after which the DNA was blotted to membrane and detected by hybridization with radioactive probe (see Materials and Methods). (a) Autoradiograph of the blot; (b) scans of selected lanes. Samples: A, no butyrate addition to cells, incubation at 0°C; B, no butyrate addition, incubation at 37°C only; C, butyrate added to cells 6 h before harvest, incubation at 0°C; D, butyrate added 6 h before harvest, incubation at 37°C only; E, butyrate added 12 h before harvest, incubation at 0°C; F, butyrate added 12 h before harvest, incubation at 37°C only. In panel a, N indicates the mobility of the nicked DNA and L indicates the mobility of the linear DNA; in panel b, M above the scans designates the mean mobility of the topoisomer distribution of sample B, and M below the scans designates the mean mobility of the distribution of sample F. As in Fig. 1 and 3, PM designates the predicted mean mobility for sample F according to Norton et al. (49); scan G illustrates how scan F would appear if its mean mobility were adjusted to that predicted mean. (c and d) Gaussian fits to the data as in Fig. 1d and e. (c) Gaussian fit to the data for sample B; (d) Gaussian to the data for sample F. The mean (± standard deviation), standard deviation about the mean (± standard deviation), and NK values are, respectively, −1.55 ± 0.06, 2.96 ± 0.05, and 312RT for panel c and −3.20 ± 0.04, 2.94 ± 0.03, and 403RT for panel d. No significant differences in goodness of fit were seen in samples from cells treated with and without butyrate.

specific activity in the butyrate-treated sample (data not shown).

Analysis of minichromosomes washed with 0.45 M NaCl. Norton et al. (49) have suggested that the unconstrained supercoiling resulting from histone hyperacetylation may exist only briefly in the cell, providing a signal for transcription activation proteins to bind. These additional proteins then reconstrain the supercoiling upon binding, resulting in no net change in constrained supercoiling even though the final structure contains hyperacetylated histones. Thus, our observation that histone hyperacetylation did not cause a substantial relaxation of nucleosomal supercoiling could have been due to the fact that following butyrate treatment, other proteins bound to the minichromosome in vivo to reconstrain those transiently released supercoils.

To investigate this possibility, we fractionated the nuclear extracts on Bio-Gel A-5m in the presence of 0.45 M NaCl. We have used this treatment previously to remove virtually all proteins from chromatin save for the core histones (42). Thus, this treatment produces a structure very similar in biochemical composition to that of Norton et al. (49) but whose assembly occurred in vivo rather than in vitro. These purified core histone-DNA complexes were then treated with topoisomerase as described above to determine the level of constrained supercoiling.

The results of such an experiment are shown in Fig. 3. Analysis of the proteins by electrophoresis in an SDS-containing acrylamide gel (Fig. 3c) demonstrates that the column isolation removed virtually all of the proteins (histone H1, viral capsid proteins VP1, VP2, VP3, etc.) from the minichromosomes except for the core histones, while analysis on an acetic acid-urea-containing gel (Fig. 3d) demonstrates that the isolated minichromosomes still contained hyperacetylated core histones. A determination of the level of constrained supercoils in the isolated core histone-DNA complexes (Figure 3, lanes A and B; results of several experiments are summarized in Table 1) demonstrates again that histone hyperacetylation has a minimal effect on the

level of constrained supercoils; the mean of the control sample (marked M at the top Fig. 3b) is nearly the same as the mean of the butyrate-treated sample (marked M at the bottom of Fig. 3b). The location of the mean predicted by the model of Norton et al. (49) for the butyrate-treated sample is indicated by PM at the bottom of Fig. 3b; this should be compared with the M at the bottom of Fig. 3b, which marks the observed mean of the butyrate-treated sample shown in Fig. 3a, lane B. Scan C in Fig. 3b represents scan B which has been shifted so that its mean is now located at the predicted mean PM. This scan provides a graphic demonstration that had the predicted shift occurred, it would have been readily detected by this method. Thus, even when all but the core histones were removed from the minichromosome, the topological change predicted by Norton et al. (49) was not observed with minichromosomes assembled in vivo.

Finally, this experiment also assesses the possible topological effects of the proteins removed by 0.45 M salt: histone H1, viral proteins, and nonhistone chromosomal proteins such as the HMG proteins. It can be seen in Table 1 (SV40, column purified, $L_{0.45M}$–$L_{0.14M}$) that minichromosomes with and without these proteins differed little in their topologies; the salt-washed minichromosome contained approximately one more negative supercoil than did the control. This minimal topological effect of removal of histone H1 and nonhistone chromosomal proteins is consistent with the findings of several other studies (30, 47, 53). However, this result contrasts with suggestions that the topological effect of H1 is substantial (22, 62).

Effect of butyrate treatment on the level of constrained supercoiling in the minichromosome of a transfected plasmid. It is possible that the lack of effect of butyrate treatment on constrained supercoiling may be due to a feature specific to SV40 (the presence of virion proteins during minichromosome assembly, etc.). To test this possibility, a similar study of the structure of the minichromosome of a transfected plasmid was performed. We have previously analyzed the topology of the minichromosome of plasmid pORAS7 following electroporation (4). The analysis was carried out on plasmid replicated in COS7 cells to ensure its assembly into a native chromatin structure.

Figure 4 shows the results of an experiment in which pORAS7 was introduced by electroporation into COS7 cells, after which a portion of the cells was treated with butyrate. Nuclei were prepared, treated with topoisomerase, and then subjected to extraction and gel fractionation of the DNA as described above. Plasmid DNA was detected by Southern blotting rather than by staining with ethidium because of the lower level of DNA. Figure 4b shows densitometer scans of the autoradiograph. Figures 4c and d demonstrate that the envelopes of the topoisomer distributions for pORAS7 are also Gaussian, as was seen for SV40 (Fig. 1d and e). Furthermore, the fits are good and the distribution widths are similar for samples treated with and without butyrate.

Sample B of Fig. 4 is the control sample treated with topoisomerase at 37°C, and the M above the scan indicates the mean of the topoisomer distribution. Sample F is a similarly treated sample from the butyrate-treated cells, with the M at the bottom of the scans marking the mean of its topoisomer distribution. As observed above for SV40, butyrate treatment causes pORAS7 to acquire, if anything, slightly more constrained negative supercoils, not substantially fewer as predicted by Norton et al. (49) (data summarized in Table 1). The PM at the bottom of the scans indicates the predicted mean for butyrate-treated sample F. To demonstrate how the predicted change would appear if it had occurred, scan G represents scan F shifted to the left so that its mean coincides with the predicted mean. It is clear from these data that hyperacetylation has not caused the predicted change in constrained supercoiling of pORAS7 chromatin which is assembled by replication in vivo. Similar results were obtained for plasmids pUC.HSO and pKP.HNO (35) (data not shown).

TABLE 2. Effect of butyrate treatment on the thermal rotational flexibility of DNA

Sample	Length (h) of butyrate treatment	L_{37}–L_0[a]	
		Predicted[b]	Observed[c]
SV40			
Nuclear extract	0 (untreated)		−1.12 ± 0.21 (5)
	6		−1.17 ± 0.28 (3)
	12	−1.7	−0.98 ± 0.32 (4)
VTC	0		−2.0 ± 0.33 (4)
	12		−2.1 ± 0.41(4)
pORAS7, nuclei	0		−1.4 ± 0.2 (2)
	12	−2.4	−1.7 ± 0.1 (2)

[a] Linking number of the sample relaxed at 37°C minus that of the sample relaxed at 0°C.
[b] The predicted value in the butyrate-treated sample is 1.7 times that of the control sample (see text).
[c] Number of determinations is given in parentheses.

Effect of butyrate on the thermal rotational flexibility of chromatin DNA. The proposal that increased histone hyperacetylation will cause a decreased interaction with nucleosome core DNA (1, 49) also suggests that another topological property of the nucleosome, i.e., the thermal rotational flexibility of the DNA, would be changed. If less DNA is being constrained by the nucleosome core, then more DNA should be free to respond to thermal changes. The topological responses of the SV40 minichromosome (2, 19, 30, 43) and VTC (43) to thermal change have been determined, and it is known from these studies that the thermal rotational flexibility of the DNA in both types of complex is considerably less than that of free DNA. In light of the suggestion (19, 43) that linker DNA connecting the cores is similar to free DNA with respect to thermal rotation, a reasonable expectation of the effect of hyperacetylation would be that 20% (see above) of the core DNA, or 0.2×146 bp = 30 bp, is freed from core constraint and able to rotate freely. The linker DNA is about 45 bp in these cells, so hyperacetylation might be expected to increase the response to thermal change by about 1.5- to 2-fold ([30 bp + 45 bp]/45 bp = 1.7).

The experiments shown in Fig. 1 to 4 include topoisomerase treatments which were carried out at both 0 and 37°C, so the thermal rotational flexibilities can be determined from these data. The flexibility values for the various complexes are presented in Table 2. The control SV40 minichromosomes (Table 2, SV40, nuclear extract) showed a level of thermal rotational flexibility similar to that seen in previous studies (2, 19, 43). The VTC shows a value which was moderately increased over that of the bulk minichromosome, a finding which has also been previously reported (43). However, butyrate treatment has virtually no effect on the rotational flexibility of either the SV40 bulk minichromosome or VTC. Similarly, pORAS7 does not show a significantly greater flexibility in the butyrate-treated sample. Finally, a study of a bovine papillomavirus-based plasmid suggests that butyrate causes a decrease in the flexibility of chromatin DNA (32). Thus, analysis of the thermal rotational flexibility of chromatin DNA suggests that histone

hyperacetylation does not result in a lessened interaction between core histones and DNA as has been proposed (1). Our results are consistent with those of numerous other studies which report only minor effects of histone hyperacetylation on nucleosome structure (reviewed in reference 16).

Effect of butyrate on nucleosome density. One manner in which the in vitro result of fewer supercoils per nucleosome could in fact be consistent with the in vivo finding of no change after butyrate treatment would be if more nucleosomes were added to the minichromosome as a result of butyrate treatment. This suggestion would also be consistent with reports that hyperacetylation facilitates nucleosome assembly in vitro (13, 49). While this explanation would seem to eliminate the intent of the model, since no net unconstrained tension would result, it nevertheless would at least resolve the apparent difference between the in vivo and in vitro results.

We used electron microscopy to test this possibility of a butyrate-induced increase in the number of nucleosomes per minichromosome. Minichromosomes in the nuclear extracts of SV40-infected cells which were grown with and without butyrate were visualized by electron microscopy (Fig. 5). Typical beads-on-a-string images were observed for both the control (Fig. 5A) and treated (Fig. 5B) samples. The mean value for the number of nucleosomes per minichromosome for the untreated sample was determined to be 26 ± 2 (Fig. 5C), a value consistent with previous studies (17, 30). Given this value for the control sample, the butyrate-treated sample would need to contain over 32 nucleosomes per minichromosome (26/0.8 = 32.5) in order to keep the total linking number constant with nucleosomes that induce a linking number change of only 0.8. Figure 5D shows that this is clearly not the case; the butyrate-treated sample contains 26 ± 2 nucleosomes per minichromosome, a value which is essentially the same as that for the control and well below the predicted mean of 32 (designated PM in Fig. 5D). Furthermore, a micrococcal nuclease digestion analysis of pORAS7 minichromosomes showed no evidence for increased nucleosome density in the butyrate-treated sample (data not shown), a result which is consistent with the findings of others (31, 45). Thus, the discrepancy between the in vitro results (49, 50) and the in vivo results described here is not due to a butyrate-induced increase in the density of nucleosomes in vivo.

DISCUSSION

We have used minichromosomes assembled in vivo to test the proposal of Norton et al. (49, 50) that nucleosomes release a portion of their constrained supercoils when their core histones become hyperacetylated. When treated in vivo with butyrate to induce hyperacetylation, neither the SV40 minichromosome (Fig. 1) nor the minichromosome of the transfected plasmid pORAS7 (Fig. 4) shows any decrease in the level of constrained supercoiling (Table 1). This discrepancy with the in vitro result of Norton et al. (49, 50) was shown not to be due to the presence of proteins in addition to core histones on the in vivo-assembled minichromosomes (Fig. 3; Table 1), to a property specific to SV40 (Fig. 4), or to assembly of more nucleosomes per minichromosome as a result of butyrate treatment (Fig. 5). Furthermore, the suggestion that histone hyperacetylation generally reduces the interaction of core histones with DNA is argued against by the finding that the thermal rotational flexibility of the chromatin DNA is not significantly affected by histone hyperacetylation (Table 2). We propose that the observation in vitro that histone hyperacetylation causes nucleosomes to release constrained supercoiling (49) does not reflect the situation in vivo. This would mean that the mechanism of gene activation involving tension release deriving from histone hyperacetylation (49) is unlikely to be valid.

There are several plausible explanations for the discrepancy between the in vitro result (49, 50) and the in vivo results presented here. One explanation may lie in the procedure used for the in vitro assembly. The model of Norton et al. (49, 50) proposes that acetylation of already assembled chromatin produces a topological change in the chromatin, yet the experimental design which they use to obtain the results involves acetylation of histones prior to assembly. Thus, their reduced ΔL may be the consequence of an effect on the assembly process and in fact may not occur upon acetylation of histones in already assembled chromatin.

A second possibility arises from the fact that the data of Norton et al. (49) derive entirely from levels of nucleosome assembly which were no more than 60% of the level of assembly of cellular chromatin. It may well be that at this subsaturating level, the structural features of the nucleosome, at least in response to hyperacetylation, are different from those of the nucleosome assembled into the context of neighboring nucleosomes in the proper proximity. Thus, this feature of hyperacetylation-reduced supercoiling may be a transient characteristic of a minichromosome in the process of assembly, one which reverts to a normal level of supercoiling when saturation is reached. One test for this possibility would be to determine whether the hyperacetylation-reduced supercoiling is still found when the in vitro assembly is extended to the saturation level found in the cell.

A third possible explanation for the discrepancy between the in vitro and in vivo results is that the sequences used are quite different; the in vitro result derives from a 207-bp sequence repeated 18 times, while our data derive from nucleosomes bound to mixed sequences of greater than 12 kbp in total length (SV40 and pORAS7). Thus, the hyperacetylation-reduced supercoiling may represent a DNA sequence-specific feature of chromatin structure which is not characteristic of cellular chromatin in general. This possibility could be tested by determining whether hyperacetylation-reduced supercoiling is a property of in vitro assembly onto other DNA sequences, both repetitive and nonrepetitive. However, whatever the explanation for the discrepancy, we feel that our direct analysis of minichromosomes assembled in vivo demonstrates that the acetylation-reduced supercoiling is not a property of nucleosomes in the cell.

A recent study by Thomsen et al. (63) reports a reduction in the level of supercoiling of a minor fraction (15%) of a transfected plasmid when cells are grown in the presence of butyrate. However, the topology of the majority of the DNA is not significantly changed, a result which in general resembles that found here. The minor relaxed fraction which they observe may reflect the length, concentration, and unusual conditions of butyrate treatment that they use. We have not investigated the possibility that their longer treatment or their protocol involving addition, removal, and readdition of butyrate causes our comparatively homogeneous minichromosome population to become more noticeably heterogeneous in topology. Finally, butyrate causes a bovine papillomavirus-based plasmid to become more negatively supercoiled in vivo (31), a result which is qualitatively consistent with that in Table 1 (SV40, Hirt extract).

The model of Norton et al. (49) seeks to relate two

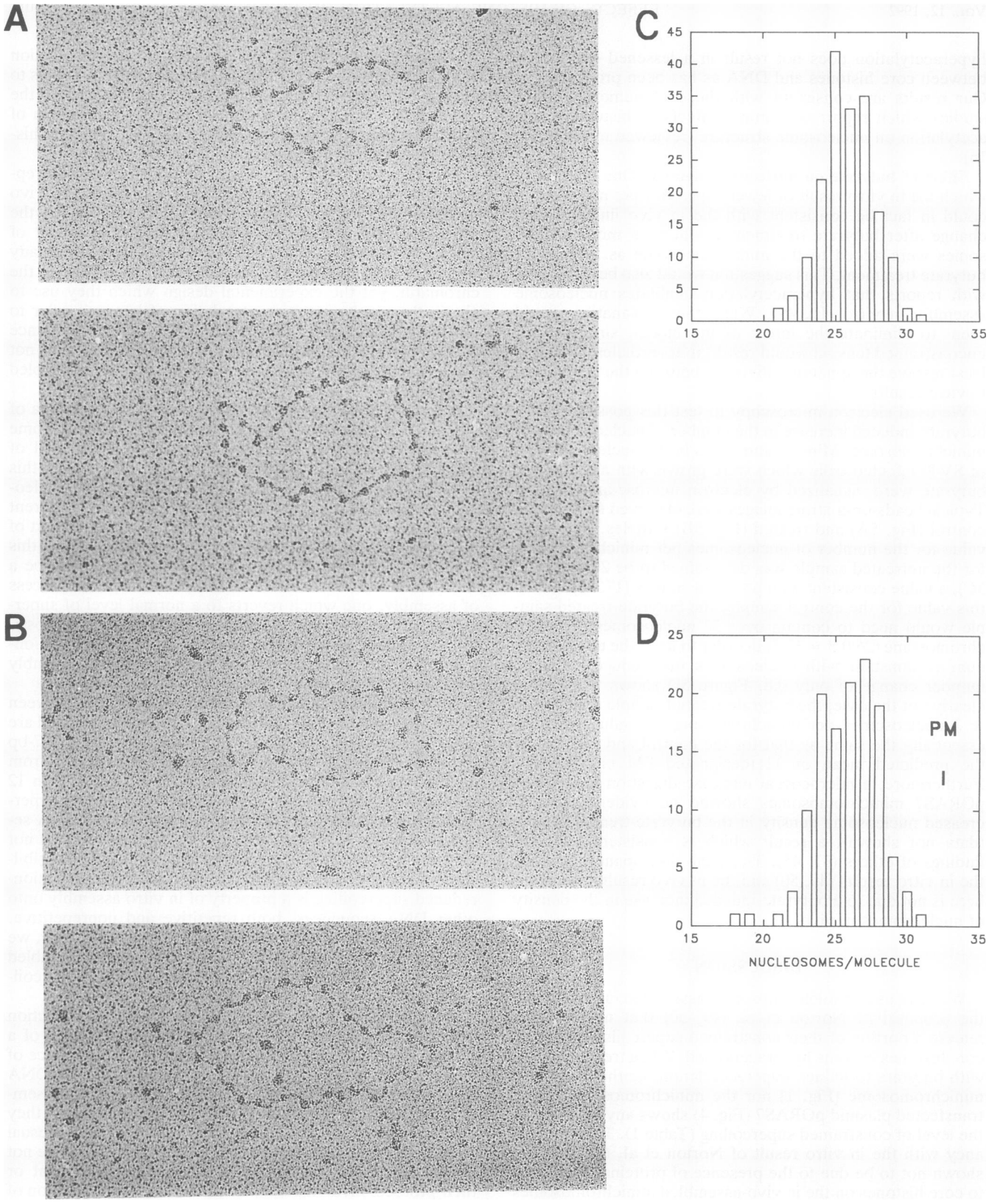

FIG. 5. Electron microscopy of SV40 minichromosomes from nuclear extract. Minichromosomes from nuclear extract of untreated cells (A) and cells grown in the presence of butyrate (B) were prepared and analyzed by electron microscopy as described in Materials and Methods. The results of counting the number of nucleosomes per minichromosome are shown in panels C (untreated) and D (butyrate treated). The data derive from two nuclear extract preparations for each type of sample. The mean ± standard deviation for panel C is 26 ± 2 nucleosomes per minichromosome (178 minichromosomes counted), while that for panel D is 26 ± 2 (173 minichromosomes counted). PM indicates the predicted location of the mean if an increase in nucleosome number were to explain the discrepancy between the in vivo and in vitro results (see text).

proposals for structural features of chromatin which regulate transcription in eukaryotes: unconstrained supercoiling and histone hyperacetylation. The likelihood that each of these proposals is true is questionable. First, the idea that unconstrained supercoiling can serve to activate eukaryotic transcription has been widely investigated, but as yet no compelling evidence has been produced in support of this contention. On the contrary, direct studies (4, 10, 11, 43, 52) have demonstrated that stable, totally unconstrained tension is clearly not a property of transcribing chromatin. While evidence for transient tension has been found to occur in the cell under special circumstances (8, 37), this is the result of transcription which is already in progress and therefore cannot play a causal role in transcriptional activation. Second, the proposal set forth originally by Allfrey (1) that histone acetylation plays a causal role in eukaryotic transcriptional activation by lessening the interaction of histones with DNA has yet to be definitively demonstrated by experimentation (for a review, see reference 16). The results from our analysis of the thermal rotational freedom of chromatin DNA (Table 2) argue against this proposal, as do a number of studies reporting minimal effects of hyperacetylation on nucleosome structure (16). Indeed, recent studies on the nucleosome whose removal is essential for hormonal stimulation of transcription indicate that hyperacetylation causes loss of transcription activation potential (6, 7). Thus, while the suggestion that acetylation induces transcription seemed plausible and likely when originally proposed, subsequent experimental results to establish this second prediction are also lacking.

ACKNOWLEDGMENTS

This work was supported by grant MV-185 from the American Cancer Society. Electron microscopy was supported by grant NSFDCB9007295 from the National Science Foundation. R.F.P. was supported by a Medical Scientist Training Program fellowship (NIGMS grant 5T32 GM67863).

We thank Christopher Drabik for providing tissue culture cells and Jeff Warmouth for photographic printing. We thank John P. Langmore, in whose laboratory the electron microscopy was performed.

REFERENCES

1. **Allfrey, V. G.** 1980. Molecular aspects of the regulation of eukaryotic transcription: nucleosomal proteins and their postsynthetic modifications in the control of DNA conformation and template function, p. 347–437. *In* L. Goldstein and D. M. Prescott (ed.), Cell biology, a comprehensive treatise, vol. 3. Gene expression: the production of RNA's. Academic Press, New York.
2. **Ambrose, C., R. McLaughlin, and M. Bina.** 1987. The flexibility and topology of simian virus 40 DNA in minichromosomes. Nucleic Acids Res. **15**:3703–3721.
3. **Boffa, L. C., G. Vidali, R. S. Mann, and V. G. Allfrey.** 1978. Suppression of histone deacetylation in vivo and in vitro by sodium butyrate. J. Biol. Chem. **253**:3364–3366.
4. **Bonilla, P. J., S. O. Freytag, and L. C. Lutter.** 1991. Enhancer-activated plasmid transcription complexes contain constrained supercoiling. Nucleic Acids Res. **19**:3965–3971.
5. **Bonner, J., G. R. Chalkley, M. Dahmus, D. Fambrough, F. Fujimura, R. C. Huang, J. Huberman, •. Jensen, K. Marushige, H. Ohlenbusch, B. Olivera, and J. Widholm.** 1968. Isolation and characterization of chromosomal nucleoproteins. Methods Enzymol. **12B**:3–65.
6. **Bresnick, E. H., S. John, D. S. Berard, P. LeFebvre, and G. L. Hager.** 1990. Glucocorticoid receptor-dependent disruption of a specific nucleosome on the mouse mammary tumor virus promoter is prevented by sodium butyrate. Proc. Natl. Acad. Sci. USA **87**:3977–3981.
7. **Bresnick, E. H., S. John, and G. L. Hager.** 1991. Histone hyperacetylation does not alter the positioning or stability of phased nucleosomes on the mouse mammary tumor virus long terminal repeat. Biochemistry **30**:3490–3497.
8. **Brill, S. J., and R. Sternglanz.** 1988. Transcription-dependent DNA supercoiling in yeast DNA topoisomerase mutants. Cell **54**:403–411.
9. **Candido, E. P. M., R. R. Reeves, and J. R. Davie.** 1978. Sodium butyrate inhibits histone deacetylation in cultured cells. Cell **14**:105–113.
10. **Choder, M., and Y. Aloni.** 1988. In vitro transcribed SV40 minichromosomes, as the bulk minichromosomes, have a low level of unconstrained negative supercoils. Nucleic Acids Res. **16**:895–905.
11. **Choder, M., and Y. Aloni.** 1988. RNA polymerase II allows unwinding and rewinding of the DNA and thus maintains a constant length of the transcription bubble. J. Biol. Chem. **263**:12994–13002.
12. **Coca-Prados, M., G. Vidali, and M. T. Hsu.** 1980. Intracellular forms of simian virus 40 nucleoprotein complexes. III. Study of histone modifications. J. Virol. **36**:353–360.
13. **Cotten, M., and R. Chalkley.** 1985. Hyperacetylated histones facilitate chromatin assembly in vitro. Nucleic Acids Res. **13**:401–414.
14. **Cousens, L. S., D. Gallwitz, and B. M. Alberts.** 1979. Different accessibilities in chromatin to histone acetylase. J. Biol. Chem. **254**:1716–1723.
15. **Cozzarelli, N. R., T. C. Boles, and J. H. White.** 1990. Primer on the topology and geometry of DNA supercoiling, p. 139–184. *In* N. R. Cozzarelli and J. C. Wang (ed.), DNA topology and its biological effects. Cold Spring Harbor Laboratory Press, Cold Spring Harbor, N.Y.
16. **Csordas, A.** 1990. On the biological role of histone acetylation. Biochem. J. **265**:23–38.
17. **De Bernardin, W., T. Koller, and J. M. Sogo.** 1986. Structure of in-vivo transcribing chromatin as studied in simian virus 40 minichromosomes. J. Mol. Biol. **191**:469–482.
18. **Depew, D. E., and J. C. Wang.** 1975. Conformational fluctuations of DNA helix. Proc. Natl. Acad. Sci. USA **72**:4275–4279.
19. **Esposito, F., and R. R. Sinden.** 1987. Supercoiling in prokaryotic and eukaryotic DNA: changes in response to topological perturbation of plasmids in E. coli and SV40 in vitro, in nuclei and in CV-1 cells. Nucleic Acids Res. **15**:5105–5124.
20. **Finch, J. T., L. C. Lutter, D. Rhodes, R. S. Brown, B. Rushton, M. Levitt, and A. Klug.** 1977. Structure of nucleosome core particles of chromatin. Nature (London) **269**:29–36.
21. **Fisher, L. M.** 1984. DNA supercoiling and gene expression. Nature (London) **307**:686–687. (news.)
22. **Freeman, L. A., and W. T. Garrard.** 1992. DNA supercoiling in chromatin structure and gene expression. Crit. Rev. Eukaryotic Gene Exp. **2**:165–209.
23. **Futcher, B.** 1988. Supercoiling and transcription, or vice versa? Trends Genet. **4**:271–272.
24. **Hadlock, K. G., and L. C. Lutter.** 1990. T-antigen is not bound to the replication origin of the simian virus 40 late transcription complex. J. Mol. Biol. **215**:53–65.
25. **Hadlock, K. G., M. W. Quasney, and L. C. Lutter.** 1987. Immunoprecipitation of the simian virus 40 late transcription complex with antibody against T-antigen. J. Biol. Chem. **262**: 15527–15537.
26. **Hagopian, H. K., M. G. Riggs, L. A. Swartz, and V. M. Ingram.** 1977. Effect of n-butyrate on DNA synthesis in chick fibroblasts and HeLa cells. Cell **12**:855–860.
27. **Hames, B. D.** 1981. Introduction to PAGE, p. 1–86. *In* B. D. Hames and D. Rickwood (ed.), Gel electrophoresis of proteins: a practical approach. IRL Press, Oxford.
28. **Hirt, B.** 1967. Selective extraction of polyoma DNA from infected mouse cell cultures. J. Mol. Biol. **26**:365–369.
29. **Keller, W.** 1975. Determination of the number of superhelical turns in simian virus 40 DNA by gel electrophoresis. Proc. Natl. Acad. Sci. USA **72**:4876–4880.
30. **Keller, W., U. Muller, I. Eicken, I. Wendel, and H. Zentgraf.** 1978. Biochemical and ultrastructural analysis of SV40 chroma-

tin. Cold Spring Harbor Symp. Quant. Biol. **421**:227–244.
31. **Krajewski, W. A., and A. N. Luchnik.** 1991. Relationship of histone acetylation to DNA topology and transcription. Mol. Gen. Genet. **230**:442–448.
32. **Krajewski, W. A., and A. N. Luchnik.** 1991. High rotational mobility of DNA in animal cells and its modulation by histone acetylation. Mol. Gen. Genet. **231**:17–21.
33. **La Bella, F., and C. Vesco.** 1980. Late modifications of simian virus 40 chromatin during the lytic cycle occur in an immature form of virion. J. Virol. **33**:1138–1150.
34. **Labhart, P., and T. Koller.** 1981. Electron microscope specimen preparation of rat liver chromatin by a modified Miller spreading technique. Eur. J. Cell Biol. **24**:309–316.
35. **Li, J. J., K. W. C. Peden, R. A. F. Dixon, and T. Kelly.** 1986. Functional organization of the simian virus 40 origin of DNA replication. Mol. Cell. Biol. **6**:1117–1128.
36. **Lilley, D. M.** 1983. Eukaryotic genes—are they under torsional stress? Nature (London) **305**:276–277. (News.)
37. **Liu, L. F., and J. C. Wang.** 1987. Supercoiling of the DNA template during transcription. Proc. Natl. Acad. Sci. USA **84**:7024–7027.
38. **Llopis, R., and G. R. Stark.** 1981. Two deletions within genes for simian virus 40 structural proteins VP2 and VP3 lead to formation of abnormal transcriptional complexes. J. Virol. **38**:91–103.
39. **Luchnik, A. N., V. V. Bakayev, and V. M. Glaser.** 1983. DNA supercoiling: changes during cellular differentiation and activation of chromatin transcription. Cold Spring Harbor Symp. Quant. Biol. **472**:793–801.
40. **Luchnik, A. N., V. V. Bakayev, A. A. Yugai, I. B. Zbarsky, and G. P. Georgiev.** 1985. DNAaseI-hypersensitive minichromosomes of SV40 possess an elastic torsional strain in DNA. Nucleic Acids Res. **13**:1135–1149.
41. **Luchnik, A. N., V. V. Bakayev, I. B. Zbarsky, and G. P. Georgiev.** 1982. Elastic torsional strain in DNA within a fraction of SV40 minichromosomes: relation to transcriptionally active chromatin. EMBO J. **1**:1353–1358.
42. **Lutter, L. C.** 1978. Kinetic analysis of deoxyribonuclease I cleavages in the nucleosome core: evidence for a DNA superhelix. J. Mol. Biol. **124**:391–420.
43. **Lutter, L. C.** 1989. Thermal unwinding of simian virus 40 transcription complex DNA. Proc. Natl. Acad. Sci. USA **86**: 8712–8716.
44. **Maniatis, T., E. F. Fritsch, and J. Sambrook.** 1982. Molecular cloning: a laboratory manual. Cold Spring Harbor Laboratory, Cold Spring Harbor, N.Y.
45. **Mathis, D. J., P. Oudet, B. Wasylyk, and P. Chambon.** 1978. Effect of histone acetylation on structure and in vitro transcription of chromatin. Nucleic Acids Res. **5**:3523–3547.
46. **Morse, R. H.** 1992. Topoisomer heterogeneity of plasmid chromatin in living cells. J. Mol. Biol. **222**:133–137.
47. **Morse, R. H., and C. R. Cantor.** 1986. Effect of trypsinization and histone H5 addition on DNA twist and topology in reconstituted minichromosomes. Nucleic Acids Res. **14**:3293–3310.
48. **North, G.** 1985. Eukaryotic topoisomerases come into the limelight. Nature (London) **316**:394–395. (News.)
49. **Norton, V. G., B. S. Imai, P. Yau, and E. M. Bradbury.** 1989. Histone acetylation reduces nucleosome core particle linking number change. Cell **57**:449–457.
50. **Norton, V. G., K. W. Marvin, P. Yau, and E. M. Bradbury.** 1990. Nucleosome linking number change controlled by acetylation of histones H3 and H4. J. Biol. Chem. **265**:19848–19852.
51. **Panyim, S., and R. Chalkley.** 1969. High resolution acrylamide gel electrophoresis of histones. Arch. Biochem. Biophys. **130**: 337–346.
52. **Petryniak, B., and L. C. Lutter.** 1987. Topological characterization of the simian virus 40 transcription complex. Cell **48**:289–295.
53. **Rodriguez Campos, A., A. Shimamura, and A. Worcel.** 1989. Assembly and properties of chromatin containing histone H1. J. Mol. Biol. **209**:135–150.
54. **Roman, A.** 1982. Alteration in the simian virus 40 maturation pathway after butyrate-induced hyperacetylation of histones. J. Virol. **44**:958–962.
55. **Ross, M. G., R. G. Whittaker, J. R. Neumann, and V. R. Ingram.** 1977. n-Butyrate causes histone modification in HeLa and Friend erythroleukaemia cells. Nature (London) **268**:462–464.
56. **Ryoji, M., and A. Worcel.** 1985. Structure of the two distinct types of minichromosomes that are assembled on DNA injected in Xenopus oocytes. Cell **40**:923–932.
57. **Schaffhausen, B. S., and T. L. Benjamin.** 1976. Deficiency in histone acetylation in nontransforming host range mutants of polyoma virus. Proc. Natl. Acad. Sci. USA **73**:1092–1096.
58. **Sealy, L., and R. Chalkley.** 1978. The effect of sodium butyrate on histone modification. Cell **14**:115–121.
59. **Shelton, E. R., P. M. Wassarman, and M. L. DePamphilis.** 1980. Structure, spacing, and phasing of nucleosomes on isolated forms of mature simian virus 40 chromosomes. J. Biol. Chem. **255**:771–782.
60. **Simpson, R. T., F. Thoma, and J. M. Brubaker.** 1985. Chromatin reconstituted from tandemly repeated cloned DNA fragments and core histones: a model system for study of higher order structure. Cell **42**:799–808.
61. **Sinden, R. R., J. O. Carlson, and D. E. Pettijohn.** 1980. Torsional tension in the DNA double helix measured with trimethylpsoralen in living E. coli cells: analogous measurements in insect and human cells. Cell **21**:773–783.
62. **Stein, A.** 1980. DNA wrapping in nucleosomes. The linking number problem reexamined. Nucleic Acids Res. **8**:4803–4820.
63. **Thomsen, B., C. Bendixen, and O. Westergaard.** 1991. Histone hyperacetylation is accompanied by changes in DNA topology in vivo. Eur. J. Biochem. **201**:107–111.
64. **Weintraub, H.** 1983. A dominant role for DNA secondary structure in forming hypersensitive structures in chromatin. Cell **32**:1191–1203.